Soil Bearing Tests Using a Spherical Penetration Device

GHULAM S. BUTT, Pakistani Army Corps of Engineers; and
TURGUT DEMIREL and RICHARD L. HANDY, Department of Civil Engineering, Iowa State University

•ALTHOUGH widely used for evaluations of strengths of soils, present bearing capacity and static penetrometer tests tend to give nonlinear relationships between load and contact area. This is usually attributed to edge punching shear, which in turn is influenced by the perimeter-area ratio. The plate bearing test, for example, may be performed with different size of plates, and results corrected for the perimeter shear effect or extrapolated to an anticipated loading area. Alternately the bearing or penetration tests are standardized at a certain size and results are used in empirical correlations; the widely used California bearing ratio is one such test.

A review of Prandtl theory for bearing-type or punching shear failure in metals and the Brinnell hardness test for metals (6) suggested that a test might be devised to eliminate or reduce this dimensional aspect of bearing testing (2). If successful, such a test would give a bearing value independent of plate or penetrometer size that might be readily converted into existing evaluations such as CBR or plate bearing k, or that might be usable directly as a bearing capacity.

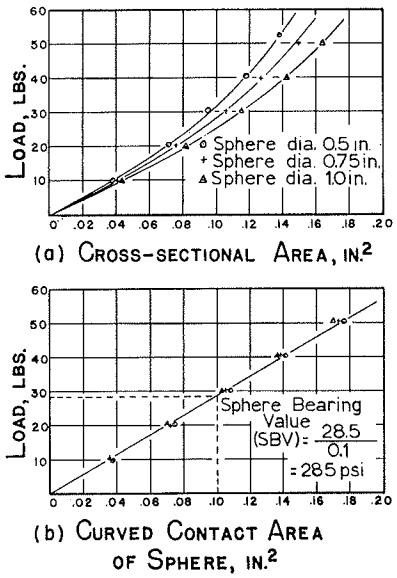

Figure 1. Relationship between load and areas of different sizes of spheres: (a) load vs cross-sectional area; (b) load vs curved contact area of sphere.

A specimen of loess silt was compacted at optimum moisture content with standard compactive effort in CBR molds. Three sizes of sphere diameters were used: 0.75 in., 0.562 in., and 0.50 in. On each specimen three tests were run, one with each sphere under similar conditions.

If the mean pressure is defined similar to the Meyers hardness number, i.e., Load/Cross Section Area of Indentation, the plot is curved as shown in Figure 1a. However, if mean pressure is defined similar to the Brinnell hardness number, i.e., Load/Contact Area, then the curve is one straight line regardless of sphere size, (Fig. 1b). For soils the pressure divided by contact area will be referred to as the Sphere Bearing Value (SBV), given here in psi; that is,

$$SBV = \frac{\text{Load}}{\text{Contact Area}} = \frac{W}{\pi Dh}$$

where W is load, D is diameter of the sphere, and h is penetration depth. (Because of the linear graph, SBV can also be expressed metrically.) Similar results were obtained by Demirel and Enustun in 1955 (2) and Tsytovitch in 1960 (10).

Paper sponsored by Committee on Soil and Rock Properties.

CLASSICAL BEARING CAPACITY THEORY

Classical bearing capacity theories in soil mechanics are modifications of theories of plastic deformation of metals. The shape of the deformation zone or the plastic flow zone plays an important role in interpretation of these theories for our purpose. It is essential to investigate the shape of the failure surfaces and determine their influence on the bearing capacity of the soil surface.

The problems of deformations of metals were studied by Prandtl (1920), Hencky (1923), Ishlinsky (1944), and others. A summary of their conclusions, without attempting a rigorous proof, is given below.

According to Prandtl and Hencky, when a load is first applied to a flat rectangular punch on metal, the shear stresses developed at the edge of the punch are very high. Consequently, even with a small applied load, these regions will be in a state of incipient plasticity. As the load on the punch increases, the material around the punch is in a state of plasticity and the indenter begins to penetrate. The failure zone is shaped like two wings and the zone is commonly known as the Prandtl failure zone. The applied load on the punch is assumed to cause a uniform normal pressure over the face of the punch and is given by $p = 5.14\ k$, where k is a constant for a metal.

This solution was adopted by Terzaghi (8) for determining the ultimate bearing capacity of continuous footings with a smooth base. The equation for this ultimate bearing capacity per unit of area is $q_o = 5.14\ C$ where C is the cohesion of the soil. The ultimate bearing capacity of soil is thus analogous to the mean pressure at in instant of full-scale plastic flow in metals.

In a similar manner Hencky and Ishlinsky have shown that the pressure needed by a circular punch to penetrate the surface of a metal equals 5.2 k to 6 k. Terzaghi modified this relation and gave the following empirical relation to determine the ultimate bearing capacity of a smooth circular footing on a purely cohesive soil: $q_o = 1.3\ (5.14\,C)$.

For deformation of metals by a spherical indenter, Ishlinsky (4, 6) determined that the mean pressure, i.e., the load divided by the cross-sectional area, has a value of about 2.66 Y, where Y is the constant yield stress of the material, analogous to the unconfined compressive strength of the soils.

MODEL INVESTIGATION OF THE DEFORMED ZONE UNDER A SPHERICAL PENETROMETER

In the theoretical treatments of bearing capacity the soil is assumed to be rigid until plastic, i.e., no significant strains occur until rupture occurs. It is also assumed that a boundary exists which encloses all material that is plastically deformed. Equations and calculations are therefore valid only to the extent that the two assumptions are approximately satisfied. Since these two assumptions are not strictly valid in soils, it is not surprising to find that the plastic theory does not provide a completely satisfactory explanation of the deformation pattern.

It was recognized that the penetration of a sphere is a three-dimensional problem where symmetry exists on any plane that includes the central axis. Deformations were examined in two planes, by contouring the surface of indented specimen, and photographing movements in a vertical section cut through the center of the indenter. For the first, specimens were molded in Proctor molds at standard Proctor compaction and various moisture contents, except that the sand was compacted dry. A line was inscribed on the surface of the specimen, and heights were measured at intervals of 1 cm along the inscribed line. A steel ball of 0.75 in. diameter was placed at the center and loaded with increments of 10 lb. After each test, the load and ball were removed and the heights remeasured to give the change in surface elevation. Any hair cracks that appeared on the surface were examined under a magnifying glass, and their lengths were measured with vernier calipers.

In the second technique, specimens were molded by static compaction in a heavy steel mold used for the ASTM soil-cement flexure beam test (1). A specimen 3 by 3 by $11\frac{1}{4}$ in. was transferred to an aluminum box of the same size having a detachable $\frac{3}{4}$-in. thick Plexiglas front. Before the front was attached, a grid was scratched on the face of the specimen and small ball bearings were embedded at the intersections. The Plexiglas

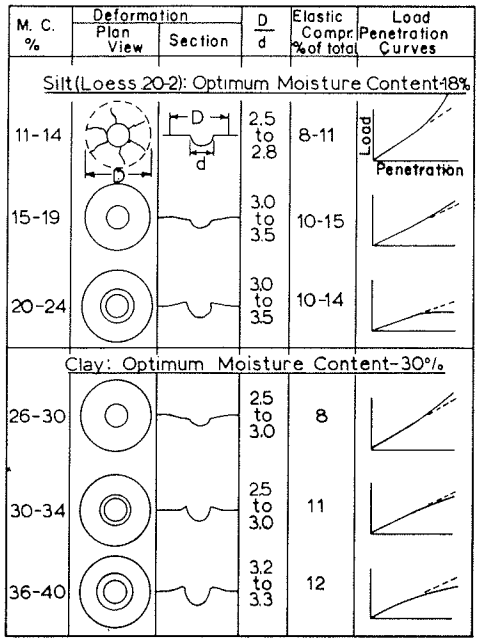

Figure 2. Deformation characteristics of silt and clay.

wall was then bolted in position to contact the specimen. A lubricated hemisphere was placed with its flat surface against the Plexiglas, in contact with the top of the specimen. The sphere was then loaded, and a series of 1-sec. time exposure photographs were taken at no load (for reference) and at various states during the process of deformation under each applied load. This technique was not highly sensitive, and a zone of small deformations could exist that might not be detected on the photographs.

Silt Deformation Analysis

Surface deformations in the silt were found to depend on moisture content, as shown in Figure 2. At a moisture content well below optimum no change of height of the specimen surface was observed except at the point of indentation, and radial hair cracks appeared on the surface of the specimen, their length increasing with increasing applied loads. The diameter of a hypothetical circle joining the extremities of these cracks was found to be 2.56 d to 2.80 d, where d is the diameter of the indentation. Elastic rebound amounted to 8 to 11 percent of the penetration. After penetration was about 15 percent of the sphere diameter, as the load increased the line curved upwards, indicating an increased resistance of soil to penetration, perhaps because of compaction.

At moisture contents between 15 and 19 percent and near optimum (18 percent) no radial cracks appeared, and the surface of the specimen around the indentation decreased in height. The area thus affected could be enclosed with a circle of diameter 3 to 3.5 times d. Close to the optimum moisture content, concentric rings of cracks appeared around the indentation, with new rings forming progressively outwards as the load increased. The slope of the load vs penetration curve was similar to that observed at lower moisture contents, and the elastic recovery ranged between 10 and 15 percent of total penetration of the sphere.

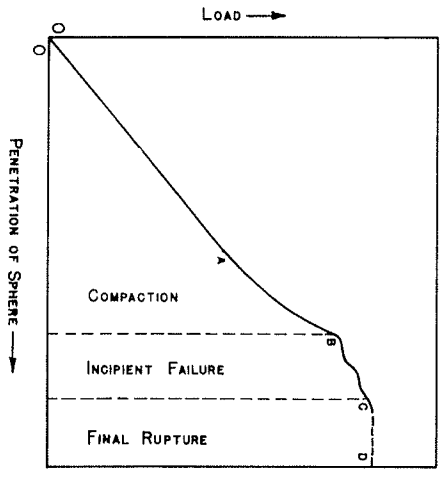

Figure 3. Stages of deformation process of soil.

At moisture contents well above optimum there was another change in deformation characteristics: the load vs penetration curves after the linear portion sloped downward, and a raised lip of soil formed around the sphere. The diameter of the raised surface was 2 to 3 times d.

Two silt specimens molded at optimum moisture content were subjected to very high loads. Initial load increments showed a straight-line relation which corresponds to 0-A in Figure 3. During the next increments the line curved upwards (A-B) showing the previously noted increased resistance of the soil to penetration. At still higher loads the curve was erratic (B-C), and finally the sphere suddenly disappeared below the surface. These stages are interpreted as representing states

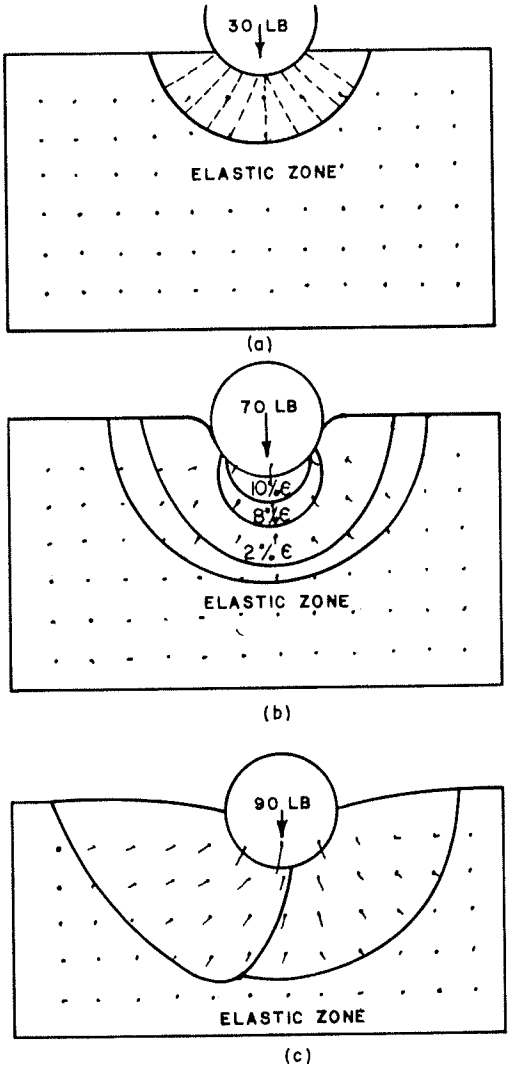

Figure 4. Stages of deformation in silt, showing (a) the flow lines, represented by dotted lines; (b) semicircular deformed area and strain contours; and (c) incipient failure conforming to one wing of a Prandtl deformation boundary.

of equilibrium compaction, incipient failure, and final rupture when shear strength of soil is completely exhausted.

Figure 4 shows the deformations in a vertical plane in loess molded at 16 percent moisture content. The deformed area of the grid is approximately semicircular with a center on the axis of the indenter following the Boussinesq pattern for major principal stresses. The dotted lines in Figure 4 are the flow lines, indicated by movements of the spheres during the time exposure photographs. The percent strain was measured and contoured; high-strain contours are nearly elliptical near the ball, merging gradually into an approximately circular plan at greater depths. The elastic-plastic boundary was sketched to enclose all detected movement.

In Figure 4c, an eccentric zone of compression has emerged, conforming to one wing of a Prandtl deformation boundary. We may assume that shear failure is incipient compounded with eccentric compression. In both Figure 4b and 4c the free surface of soil is depressed, and the ratio D/d is in close agreement with observations in the first series of tests. The ratio of curved area of the elastic-plastic boundary to sphere contact area ranged between 6.7 and 7.4.

Clay Deformation Analysis

The optimum moisture content of the clay at standard Proctor density is 30 percent, and specimens were molded with moisture content ranging from 26 to 40 percent. Specimens molded below 26 percent were discarded because of a honeycombed texture.

The clay surface geometry was almost identical to that observed in silt at ranges of moisture content around the optimum (Fig. 2). The ratio D/d is approximately 3. The load vs penetration curves at moisture contents below and close to optimum deviate very little from a straight line even at higher loads. Figure 5 shows deformations in a vertical plane in the clay sample molded at 30 percent moisture content. The pattern of deformation in Figure 5a is again radial, with a hemispherical elastic-plastic boundary. The ratio of this boundary area to sphere area is 6.6.

Figure 5 shows a failure pattern approximating Prandtl-type failure zones. However, below the failure zone a zone of radial compression extends in a somewhat hemispherical form, probably distorted by the confines of the box. There is also bulging of the free surface adjacent to the sphere.

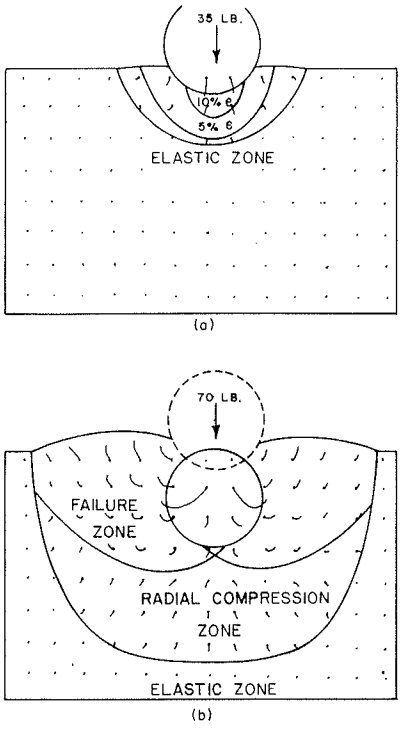

Figure 5. Stages of deformation in clay, showing (a) radial compression, and (b) Prandtl-type failure zones and radial compression zone extending up to the elastic zone.

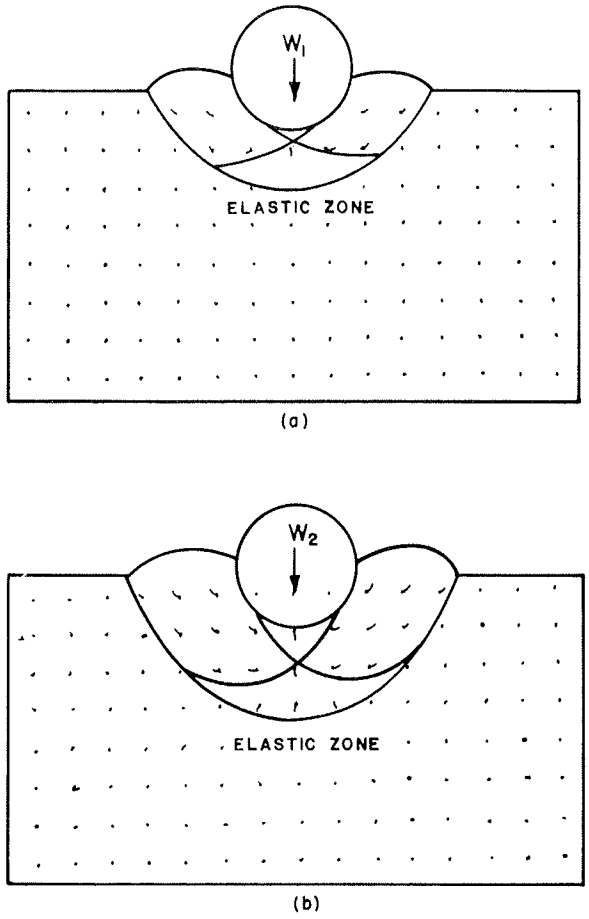

Figure 6. Deformation boundaries in sand with increasing applied loads. Rupture surfaces are curved and sliding takes place in a rotary motion.

Sand Deformation Analysis

Dry compacted sand was used in a series of tests. Because of weakness of the sand it was not possible to take an initial zero reading; therefore observations were entirely qualitative.

As seen in cross section, the sand particle movement initially was vertically downward. As settlement of the sphere increased, the soil was displaced laterally along slip surfaces. These slip surfaces curved upward to reach the free surface of soil around the sphere and form a mound, as seen in Figure 6. The rupture surfaces are curved, and sliding takes place in a rotary motion. Approximate failure planes and elastic-plastic boundaries are sketched in Figure 6. As in clay, there is a deep-rooted zone of compression underneath the shear surfaces.

Discussion

The experimental evidence indicates that penetration of a soil mass by a spherical penetrometer occurs in two stages: compression of soil, and rupture of soil by plastic flow combined with deep compression.

Compression—Prior to application of load on the soil surface the soil mass is in elastic equilibrium. When the load is applied on a sphere, there is a uniform radial displacement and compression of soil which causes a change in volume by densification. In permeable soil the decrease in volume is rapid and results in downward deflection of

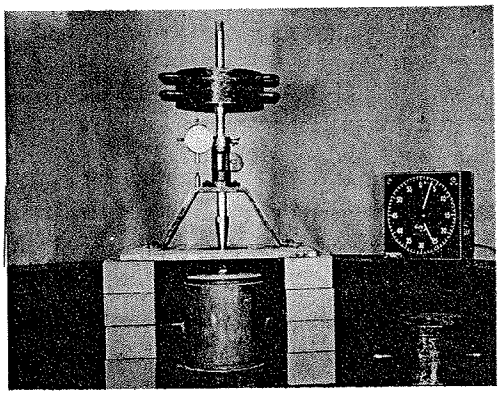

Figure 7. Spherical penetrometer used in laboratory investigations.

the surface of the specimen around the indenter. In turn, densification causes a decreased porosity and an increased resistance to penetration, whereas in theoretical treatments it is assumed that the material is incompressible and there is no volume change throughout the process of deformation.

The mechanism of deformation may be regarded as essentially compression of a set of concentric hemispherical shells except in a region very close to the sphere, where densification probably forms a cap of dead soil. Outside this cap, the irregularities of strain are rapidly smoothed out and an approximately uniform radial strain is produced.

Flow—The onset of plastic flow is preceded by irregular settlement under an increasing load. In some cases the curved rupture surface is eccentric. In most cases, because the sphere is centrally loaded, symmetrical doughnut-shaped rupture takes place beneath the sphere. In all the three soils tested, an inverted cone of soil was visible at this stage, the base of the cone being against the sphere. Initially the cone is short, but as the sphere penetrates deeper and the contact angle increases the cone becomes larger. The rupture surfaces and the flow lines are curved, rising up to a free surface of the soil.

At higher moisture contents the load vs penetration curve falls below the initial straight line, and a mound of soil appears around the sphere. It is reasonable to assume that at this stage the shear strength of soil is completely exhausted; the strains are large compared to stresses imposed, the deformation zone is in a state of plastic flow. The point at which slope of curve changes is the ultimate bearing capacity of soil.

The theoretical treatment also assumes that deformation is entirely within a boundary described by a rupture surface. It appears, from this investigation, that this boundary does not enclose the full plastic region, since there is a further zone in which the material is pseudo-elastically compressed. Here the compression and the plastic parts of the strain may be of comparable magnitude.

None of the plastic-elastic boundaries determined in the soil models correspond exactly to those of the theoretical models, a fact recognized by Terzaghi (8).

LABORATORY AND FIELD TESTS

The laboratory test device (Fig. 7) consists of a sphere, a loading frame, and a dial gage to measure the depth of penetration. Specimens were molded in CBR molds at different moisture contents and compactive energies. At least five tests were conducted on each sample to obtain load vs sphere contact area curves. The SBV is the slope of the line, and is expressed in psi.

One advantage of a linear load to area relationship is that fewer readings are needed to establish a line. To fully exploit this advantage and save time, a "one-shot" method was tried whereby only one load and its corresponding penetration was used to find the bearing value. The initial contact between the sphere and the soil was indicated by an electrical circuit.

Sphere bearing tests were performed on one face of the CBR specimens and CBR tests were performed on the opposite faces of the specimens. Triaxial compression tests, unconfined compressive strength tests, and direct shear tests were also performed to correlate with the SBV. The laboratory tests were performed on a loess silt, a montmorillonite clay, and a sand; their properties are given in Table 1.

Field tests were performed on a silty clay, a glacial till, and a sandy loam (Table 2). Since the soil in the field was heterogeneous and often had large pebbles, small diame-

TABLE 1
PROPERTIES OF SOILS TESTED IN THE LABORATORY

Property	Clay	Loess 20-2	Sand
Physical properties			
Liquid limit, %	88.8	30.8	—
Plastic limit, %	30.1	24.6	—
Plasticity index, %	58.7	6.2	NP
Specific gravity	2.74	2.71	—
Textural composition			
Gravel (2 mm)	—	—	
Sand (2-0.074 mm)	0.5	0.4	100
Silt (0.074-0.005 mm)	9.0	79.8	—
Clay (<0.005 mm)	90.5	19.8	—
Colloidal clay (<0.001 mm)	35.0	14.5	—
Field dry density, pcf	93.2	83.3	—
Field moisture content, %	33.0	17.0	—
Textural classification (BPR system)	Clay	Silty loam	Sand
AASHO-ASTM classification	A-7-6(20)	A-4(8)	A-1-a

ter spheres gave erratic values, and field penetrometers were made with 12 and 6-in. diameters. The loading device consisted of a hydraulic jack with 10,000-lb capacity, equipped with a gage graduated in increments of 200 lb. This was connected to the frame of a loaded truck with a ball swivel. Prior to testing, the top 6 in. or more of desiccated soil was removed from an area 3 by 3 ft and the area was leveled and smoothed with a hand trowel. The equipment was set up as shown in Figure 8. Five equal load increments were applied, and the penetration for each increment was recorded to give load vs contact area curves.

"One-shot" load tests were also performed in the field, and the values obtained were only slightly different from those obtained by the method described above. In no tests did total penetration exceed 15 percent of the diameter of the sphere, which is regarded as a limiting value for the load-contact area proportionality.

The field sphere bearing tests were correlated with the modulus of subgrade reaction obtained from the plate bearing tests with a 12-in. diameter plate and the ultimate bearing capacity of soil using values of C and φ obtained with the field bore-hole shear device (3) and triaxial compressive tests.

Correlation and Comparison Test Results

SBV vs CBR—One of the objectives of the investigation was to establish, if possible, a relationship between the SBV and the CBR.

TABLE 2
PROPERTIES OF SOILS—FIELD TESTS

Property	Silty Clay	Glacial Till	Sandy Loam
Physical properties			
Liquid limit	61.4	24.0	—
Plastic limit	26.1	15.0	NP
Plasticity index	35.3	9.0	—
In-place density, pcf	126.9	138.0	83.7
Dry density, pcf	99.5	125.8	78.8
Field moisture content, %	27.3	10.2	6.23
Textural composition			
Gravel (>2 mm)	—	4.2	8.6
Sand (2-0.074 mm)	24.0	42.9	66.4
Silt (0.074-0.005 mm)	24.6	28.7	14.9
Clay (<0.005 mm)	51.2	24.2	20.1
Colloidal clay (<0.001 mm)	44.1	17.5	9.3
AASHO-ASTM classification	A-7-6(20)	A-4(4)	A-2-4(0)

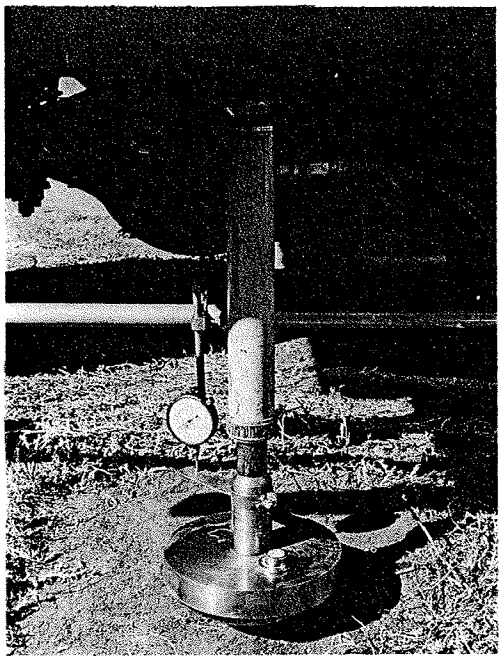

Figure 8. Field spherical penetrometer with 12-in. diameter.

Statistical analysis of the data gave a coefficient of variation of 0.142 (14.2 percent) for the CBR tests and 0.0767 (7.67 percent) for the sphere bearing tests, or about half. This indicates that an individual sphere bearing test is more reliable and reproducible than a CBR test. Consistency of the sphere bearing test was also observed in the field tests (Table 3).

All comparative CBR and SBV data are shown in Figure 9. Since most of the tests were on loess, a regression line and 95 percent confidence band were drawn for the loess tests, omitting those at very low moisture content (x's in Fig. 9) and those at very high moisture content (grouped near the origin). The tests on clay fell on or near the same regression line, but those on sand did not. Much of the width of the confidence band probably relates to the lower reproducibility of the CBR tests.

Apparently when the moisture content is low, soil under the sphere densifies and offers increased resistance to penetration—more so than under a flat piston—giving a higher SBV in relation to the CBR. At high moisture contents the CBR value is higher than the corresponding SBV, probably because of viscous resistance, since the CBR test utilizes a higher rate of shear.

In the case of the sand, all CBR tests were performed with a 10-lb surcharge on the specimen, whereas all the sphere bearing tests were performed without any surcharge. Since coehesionless sand does not develop any resistance to deformation unless it is confined and/or loaded over a large area, the sand CBR test values shown in Figure 9 are much higher than the corresponding SBV's. The SBV's of these tests are merely an indication of the bearing capacity without surcharge.

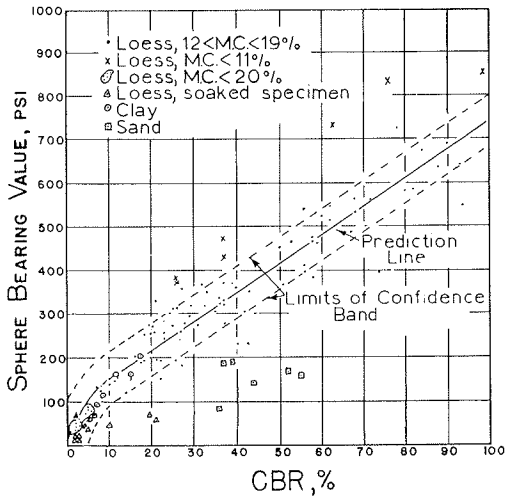

Figure 9. Relationship between the sphere bearing value and the CBR.

No relationship was found between the sphere bearing test data and the corresponding CBR ratings of the soaked specimens. The data, however, are also plotted in Figure 9. After a specimen had been soaked for four days, its surfaces became very soft and did not offer much resistance to penetration of the sphere.

To sum up, a correlation exists between the SBV and the unsoaked CBR of clay and silt compacted near the optimum moisture content, and may be expressed by the following prediction equation:

$$\text{CBR, \%} = \frac{1}{6.6}\,(\text{SBV} - 84)$$

The equation does not apply to sand, or wherever the soil moisture content is far from optimum.

TABLE 3

FIELD DATA: SBV, PLATE BEARING TEST, AND BORE-HOLE SHEAR TEST RESULTS

Test No.	Soil	In-Place Dry Density, pcf	Sphere Bearing Value, psi			Plate Bearing Test		Bore-Hole Shear Test	
			12 In.	6 In.	0.75 In.	$k = \sigma/0.5$, pci	Failure Stress[a], psi	C, psi	φ
Rest area—Hwy. 69									
1	Sandy loam	98.5	55	—	—	170	48	0.5	38
2	Sandy loam	98.5	86	—	—	260	49	1.0	38
3	Sandy loam	98.5	90	94	87	250	51	1.0	38
4	Sandy loam	98.5	85	70	82	220	61	1.0	38
5	Gravelly sandy loam	98.5	115	118	—	420	52	—	—
6	Gravelly sandy loam	98.5	108	118	—	300	40	—	—
7	Gravelly sandy loam	98.5	190	157	—	—	—	—	—[b]
			200	185					
Hwy. 35—Under construction									
8	Glacial till	130	118	—	—	400	51	2.1	32
9	Glacial till	130	150	150	—	450	—	2.1	32
			150	140					
			140						
10	Glacial till	130	150	175	103	360	51	2.1	32
				175					
11	Glacial till	130	120	120	—	440	59	2.1	32
12	Glacial till	130	175	175	181	560	37	3.5	32
				200					
13	Glacial till	130	203	300	—	600	67	3.5	32
				335					
14	Glacial till	130	200	250	—	550	75	3.5	32
				300					
15	Glacial till	130	175	175	—	450	42	3.5	32
			175	205					
16	Glacial till	130	170	175	—	—	—	3.5	32[c]
			170						
County road—north of Ames									
17	Silty clay	85	70	72	—	300	57	9.2	2
18	Silty clay	85	68	—	—	360	71	9.2	2
19	Silty clay	85	75	96	—	—	—	9.2	2
				96					
20	Silty clay	85	70	60	—	—	—	9.2	2[d]
			60	60					

[a]As shown in Figure 10.
[b]Direct shear test values from Shelby-tube samples were C = 4 psi and φ = 38.
[c]UCS = 46.6 psi.
[d]UCS = 25.7 psi.

Sphere Bearing Test vs Plate Bearing Test—Small loads on a circular plate cause a settlement approximately proportional to the applied load, as shown in Figure 10. However, as the load is increased, a point is reached beyond which the settlement increases

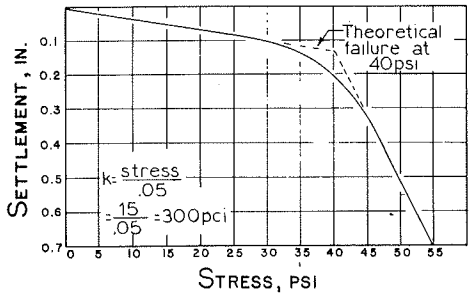

Figure 10. Stress-settlement curve of the plate bearing test.

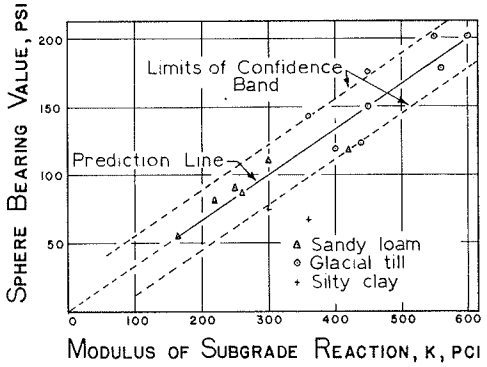

Figure 11. Relationship between SBV and k.

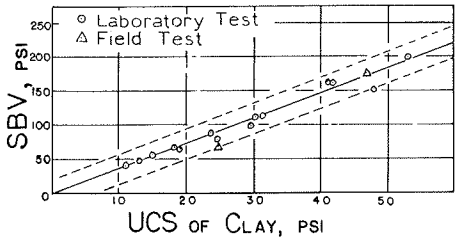

Figure 12. Relationship between SBV and UCS of clay.

much more rapidly. The initial straight-line part of the stress-deflection curve is attributed to pseudo-elastic distortion and compression of the soil, and the steep part is believed caused by shear failure. Between is a transition region of local cracking or partial failure. The intersection of two tangents, one drawn to the elastic branch of the curve and a second drawn to the steep branch, defines the theoretical point of soil failure, or the maximum load that the soil can carry (5, p. 538).

Rigid pavement designs for highways and airports are based on modulus of subgrade reaction k. Foundations are often designed on the failure-point criterion of plate bearing tests.

The numerical values of the sphere bearing test and the 12-in. circular plate tests performed in the field are given in Table 3. No correlation was found between the SBV and the plate bearing failure stress. The SBV's were much higher, probably because of the densification previously mentioned. At lower stresses an excellent linear relationship was found between SBV and the modulus of subgrade reaction k. The equation of the prediction line is

$$k = 3.0\,(SBV)$$

where k is the modulus of subgrade reaction of soil in psi/in. with a 12-in. diameter plate, and the sphere bearing value is in psi. The 95 percent confidence band and the prediction line are shown in Figure 11. In Table 3 the k values are far less reproducible than SBV, and tests repeated on the same soil give widely different values. As in the correlation with CBR, the width of the confidence band is due more to the variability of plate bearing test than the sphere bearing test.

TABLE 4

ULTIMATE BEARING CAPACITY OF SOIL BY TERZAGHI'S EQUATION FOR CIRCULAR FOOTINGS

Test No.	Soil Classification	C, psi	φ	γ, pcf	q_D, psi	SBV, psi
Field 1	Sandy loam	0.5	38	98.5	46.5	55
2	Sandy loam	1.0	38	98.5	88.0	86
3	Sandy loam	1.0	38	98.5	88.0	92
4	Sandy loam	1.0	38	98.5	88.0	80
7[a]	Sandy loam	4.0	38	98.5	340.0	183
8	Glacial till	2.1	32	130	120.0	118
9	Glacial till	2.1	32	130	120.0	146
10	Glacial till	2.1	32	130	120.0	167
11	Glacial till	2.1	32	130	120.0	120
12	Glacial till	3.5	32	130	197.0	183
13	Glacial till	3.5	32	130	197.0	203
14	Glacial till	3.5	32	130	197.0	200
15	Glacial till	3.5	32	130	197.0	175
16	Glacial till	3.5	32	130	197.0	172
17	Silty clay	9.2	2	85	69.4	71
18	Silty clay	9.2	2	85	69.4	68
19	Silty clay	9.2	2	85	69.4	89
20	Silty clay	9.2	2	85	69.4	65
Lab 178[b]	Clay	43.55	—	123	322	308
179[b]	Clay	47.8	—	116	362	346
180[b]	Clay	6.55	—	113	48.5	50

[a] C and φ values were obtained from Shelby-tube samples in lab by direct shear.
[b] C values were obtained from remolded specimens by direct shear; the remaining C and φ values were obtained in the field by the bore-hole shear device.

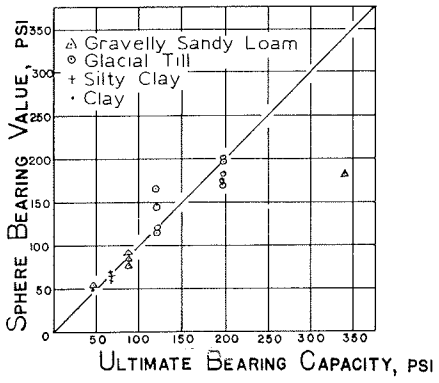

Figure 13. Relationship between the SBV and the ultimate bearing capacity of soil as determined by Terzaghi's equation for circular footings.

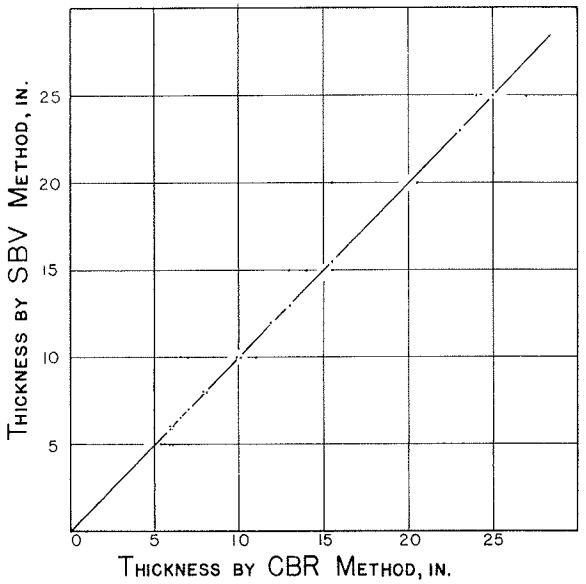

Figure 14. Relationship of pavement thickness for wheel load 9,000 lb by SBV and CBR curves.

Sphere Bearing Test vs Unconfined Compressive Strength—In cohesive soils a simple and direct determination of the ultimate bearing capacity of footings at the surface of cohesive soils has been worked out independently by Prandtl, Fellenius, and Terzaghi with fairly good agreement between their solutions. Taylor (7) has simplified their solutions in terms of unconfined compressive strength (UCS) as

$$q_u = 3.5 \text{ Unconfined Compressive Strength}$$

where q_u is the ultimate bearing capacity of circular or square footings.

In an earlier section it was shown that the mean pressure over the surface of a spherical indenter over the region of contact with metal has a value of about 3y, where y is the constant yield stress of the metal. Yield stress of the metals may be considered analogous to the unconfined compressive strength of soils. It was also observed that the shape and extent of deformation was remarkably similar to that described by Ishlinsky in the deformation of metals.

Figure 12 shows the SBV plotted against the unconfined compressive strength of clay. The regression line has the equation SBV = 3.66 UCS. The 95 percent confidence band is narrow and all the points fall within this band. For a $\varphi = 0$ soil the Terzaghi equation (discussed below) gives $q_D = 1.3\,C\,(5.7) = 7.4\,C = 3.7$ UCS, which is in excellent agreement with the observed regression values.

SBV and the Ultimate Bearing Capacity—Whereas the above equations are suitable for metals or cohesive soils, most soils also have an internal frictional component, which is included in Terzaghi's bearing capacity equation. Cohesion and φ's of the soils were measured in the field with the recently developed bore-hole shear test device (3), and ultimate bearing capacities were computed according to the equation developed by Terzaghi (9, p. 172) for circular foundations. The surcharge term was dropped from the equation because surcharge was essentially zero. To simplify the calculation, size of the footing, which has only a small effect on the bearing capacity of cohesive soils, was taken as 1 sq in. Calculated bearing values are given in Table 4 along with the SBV obtained at the test sites in three different soils. Three sets of laboratory data have also been included.

In Figure 13 the calculated bearing capacity is plotted against the sphere bearing value. A regression line may be sketched in at 45-deg, and all the points lie about this

line except for a gravelly-sandy loam. The C and φ values for this site were obtained from Shelby-tube samples by direct shear tests in the laboratory, and the value of C of 4 psi (Tables 3 and 4) appears too high. The data thus indicate that the sphere bearing value represents a reliable ultimate bearing capacity of soils with the exception of clean sands.

The correlation between SBV and theoretical bearing capacity is far better for the sphere than for the plate (Table 3), the plate bearing failure stresses for all except the weakest soil being too low. This may be partly due to the difficulty in drawing two meaningful tangents to a continuously curving line, or it may relate to densification under the sphere, as previously discussed. If the latter, the densification must be closer response to applied normal pressure, perhaps because of better drainage and lower pore pressures under the sphere than under the plate.

PAVEMENT DESIGN METHOD FROM THE SBV

The most common cause of pavement structural failure comes from increased deformation of the subgrade through repeated application of load, with consequent failure of the layers above. By application of Boussinesq theory one can derive an equation for pavement thickness Z (11)

$$Z = \left[\frac{P/p\pi}{\left(\frac{p}{p - SBV} \right)^{2/3} - 1} \right]^{1/2}$$

where P is load and p is the tire pressure.

Pavement thicknesses were calculated and compared to those from the CBR method assuming a wheel load of 9,000 lb and a uniform tire pressure of 75 psi. Pavement thicknesses were obtained by both the CBR and the SBV method for all the test data in this investigation, and a close correlation was found between the CBR design thickness and SBV design using a factor of safety of 5.5 (Fig. 14). Since the SBV test is faster (particularly the "one-shot" test) and gives better reproducibility, it might be considered for pavement design; the main limitation is in regard to clean, dry sand. This problem can be solved with further research. Also an advantage that might be exploited in future research is the adaptability of the SBV to repeated loading and the possibility for electrical monitoring of the sphere contact area.

CONCLUSIONS

1. Use of a spherical penetration test on a variety of cohesive soils gave linear plots of spherical contact area vs load. The slope of this plot is termed the sphere bearing value (SBV), dimensionally FL^{-2}, for example, psi. The sphere bearing value was found to be the same regardless of the size of the sphere, so long as the sphere is large enough to overcome inhomogeneities in the soil. An exception was clean sand, which gave nonlinear relationships, perhaps because of immediate plastic bearing capacity failure from lack of a surcharge.

2. Model tests indicated that with increasing loads, penetration of the sphere initially involves pseudo-elastic compression of cohesive soils followed by a plastic bearing capacity failure. The latter failure zone overlies zones of further compression. During the late stages of compaction and during shear failure the load-contact area plot became nonlinear after the penetration depth had exceeded 15 percent of the diameter of the sphere. The low-range load and contact area values are therefore used to determine the SBV.

3. The qualitative observation that the SBV test involves pseudo-elastic compaction was supported by a correlation between SBV and the modulus of subgrade reaction determined from the plate bearing test. A regression line indicated that $k = 3.0$ SBV, where k is in psi/in., using a 12-in. diameter plate, and the SBV is in psi.

4. The SBV also correlated with bearing capacity values such as CBR and plate bearing with several exceptions: The correlation to CBR did not hold for sands, or for silts

except near the optimum moisture content. The correlation to plate bearing failure stress did not hold for high bearing capacity soils, probably because of excess pore pressure in the plate test or imprecision in determination of the plate bearing failure point.

5. The SBV correlated closely with bearing capacities predicted from the Terzaghi equation using soil shear strength parameters C and φ obtained by use of the field borehole shear test. Plate bearing test data did not correlate nearly as well, probably for reasons mentioned in the previous conclusion.

6. A regression line gave SBV = 3.66 times unconfined compressive strength, which is very close to theoretical values.

7. An SBV flexible pavement design method based on an assumed Boussinesq vertical stress distribution and using a factor of safety of 5.5 gave pavement thicknesses comparable to those obtained by existing CBR methods.

8. Advantages of the SBV for bearing tests of soils exclusive of clean sands include

- Possibility for a more rapid "one-shot" test since the load-contact area relationship is a straight line.
- Lower coefficient of variation, i.e., better reproducibility of test results than in CBR and plate bearing testing of the same soils.
- Possibility for changing the sphere size to fit the soil or the loading equipment available with no change in SBV.
- Adaptability for repeated loading and electrical monitoring.

ACKNOWLEDGMENT

This research was done at the Engineering Research Institute, Iowa State University. The project was sponsored by the Iowa Highway Research Board, and was supported with funds from the Iowa State Highway Commission.

REFERENCES

1. Making and Curing Soil-Cement Compression and Flexural Test Specimens in the Laboratory. ASTM Standards Part 2, Designation D 1632-63, p. 476-485, 1966.
2. Demirel, T., and Enustun, B. V. Turkish Report on Soils. Perm. Internat. Assoc. Road Congress Repts. 10, 2, p. 1-14, 1955.
3. Handy, R. L., and Fox, N. S. A Soil Bore-Hole Direct-Shear Test Device. Highway Research News 27, p. 42-51, 1967.
4. Ishlinsky, A. J. Analysis of Spherical Indentation (translated title). Prikl. Matem. i Mekh. SSSR 8, No. 3, p. 233-253, 1944. Original available but not translated, cited in Tabor, D. The Hardness of Metals. The Clarendon Press, Oxford, England, p. 48, 1951.
5. Leonards, G. A., ed. Foundation Engineering. McGraw-Hill Book Co., Inc., 1962.
6. Tabor, D. The Hardness of Metals. The Clarendon Press, Oxford, England, 1951.
7. Taylor, D. W. Fundamentals of Soil Mechanies. John Wiley and Sons, Inc., 1948.
8. Terzaghi, K. Theoretical Soil Mechanics. John Wiley and Sons, Inc., 1948.
9. Terzaghi, K., and Peck, R. B. Soil Mechanics in Engineering Practice. John Wiley and Sons, Inc., 1949.
10. Tsytovitch, N. A. Bases and Foundations on Frozen Soil. HRB Special Report 58, p. 32-35, 1960.
11. Butt, G. S. Soil Bearing Tests Using a Spherical Penetration Device. Unpublished PhD thesis, Iowa State University, 1967.